

Efficient DMP generalization to time-varying targets, external signals and via-points

Antonis Sidiropoulos¹ and Zoe Doulgeri¹

Abstract—Dynamic Movement Primitives (DMP) have found remarkable applicability and success in various robotic tasks, which can be mainly attributed to their generalization and robustness properties. Nevertheless, their generalization is based only on the trajectory endpoints (initial and target position). Moreover, the spatial generalization of DMP is known to suffer from shortcomings like over-scaling and mirroring of the motion. In this work we propose a novel generalization scheme, based on optimizing online the DMP weights so that the acceleration profile and hence the underlying training trajectory pattern is preserved. This approach remedies the shortcomings of the classical DMP scaling and additionally allows the DMP to generalize also to intermediate points (via-points) and external signals (coupling terms), while preserving the training trajectory pattern. Extensive comparative simulations with the classical and other DMP variants are conducted, while experimental results validate the applicability and efficacy of the proposed method.

Index Terms—Dynamic Movement Primitives, Programming by Demonstration

I. INTRODUCTION

DYNAMIC Movement Primitives (DMP) has emerged as a promising method for encoding a desired trajectory and generalizing it to new situations. It is particularly favoured thanks to its ease of training, generalization and robustness properties and has been applied in a plethora of practical robotic tasks and applications. The trajectory to be encoded is typically provided through PbD (Programming by Demonstration) [1], as an intuitive and efficient means of teaching human-skills to robots.

In DMP, the objective of generalization is to generate a trajectory from a new initial position to a new, possibly time-varying, target position, while also preserving the shape of the demonstrated trajectory. To this end, different types of generalization have been proposed with the most well-known being the one introduced in [2]. This scaling has some important shortcomings, i.e. over-scaling of the generalized trajectory when the demonstrated end-points (initial and final position) are close, failure to generate a motion when the new end-points during execution coincide and mirroring of the trajectory when the sign of the difference between the new end-points is different from the sign of the difference of demonstrated ones. Other DMP variants that attempt to tackle the negative scaling effects include [3] and [4]. However, [3] can still produce large spatial scalings and cannot generate a motion when the new initial and final positions are the

same, while [4] fails to reproduce the demonstrated trajectory pattern to new targets that are relatively far away from the demonstrated one.

Apart from the scaling issues of DMP, generalization to via-points and taking into account within the generalization the effect of external signals has not been addressed. Via-points could be specified for instance to locally adjust a part of the DMP trajectory. Via-points with DMP were used in [5], but required also specifying the velocity and acceleration of the via-point. This can introduce significant noise, which is even more adverse if the via-points are sparsely arranged, as shown in [6]. Via-points were also included, in an offline optimization though, in a DMP-like variant in [7]. Other methodologies, such as ProMP [8], are also capable of including via-points, but are beyond the scope of DMPs that are studied here.

Coupling terms are usually employed in DMPs to adjust its trajectory to external signals, e.g. forces arising from contact with the environment or physical interaction with a human or even virtual forces like the repelling forces for avoiding limits or obstacles. Adaptation of a DMP trajectory to external signals has been studied in various works [4], [9]–[11]. However, in all these works, this external signal can significantly alter the shape of the trajectory. Enabling adaptation to such external signals, while also preserving the shape of the demonstrated trajectory is not addressed. A different approach to incorporate external signals by learning an additional coupling term through ILC (Iterative Learning Control) was investigated in [12]. However, learning required multiple repetitions of the task and these additional learned coupling terms are not accounted for in the DMP generalization.

This work exploits the novel DMP formulation presented in our previous work [13] to achieve online generalization of Dynamic Movement Primitives not only w.r.t. new initial and/or target poses but also w.r.t. via-points and/or external signals (coupling terms), while preserving the shape of the demonstrated motion. At the same time, this novel generalization approach remedies the shortcomings of the classical DMP spatial scaling. An additional perk of the proposed method is that it ensures a smooth trajectory generation, even if the provided target is discontinuous, guaranteeing that the target is reached within a prespecified desired time duration. Finally, the proposed novel generalization can also be combined with our previous work [14] to impose kinematic inequality constraints. In [14], using the DMP formulation from [13] with the classical DMP spatial scaling, an optimization framework was designed that minimizes the distance from the unconstrained scaled trajectory subject to robot kinematic inequality con-

¹Aristotle University of Thessaloniki, Department of Electrical and Computer Engineering, Thessaloniki 54124, Greece. antosidi@ece.auth.gr, doulgeri@eng.auth.gr

straints, obstacle constraints and via-points. The combination of this work with [14] improves the generalization of the generated motion under kinematic constraints as showcased through simulations.

The rest of this paper is organized as follows: In Section II we provide the preliminaries for the novel DMP formulation from [13]. Section III is devoted to the proposed novel online generalization method. Simulations that demonstrate how the proposed method works and comparisons with the classical DMP are provided in section IV. The practical usefulness and efficacy of the proposed method is further showcased in the experimental Section V. Finally, we draw the conclusions in Section VI. The source code for all conducted simulations and experiments can be found at github.com/Slifer64/novel_dmp_generalization.git.

II. DMP FORMULATION

Here we expound on the DMP formulation, which is based on the our previous DMP formulation [13], but differs principally in the way that generalization is achieved. In [13] we employed the same spatial generalization mechanism that the original DMP [2] use. This generalization is known to be problematic in some cases, resulting in large spatial scaling and in turn large velocities and accelerations, it can cause undesired mirroring of the motion and fails to produce a motion if the initial and target position coincide [4]. The proposed formulation solves all these issues and it further allows us to achieve generalization and adaptation to time-varying targets, external signals and/or via-points, guaranteeing a smooth trajectory generation.

Consider the state $\mathbf{y} \in \mathbb{R}^n$, which can be joint positions, Cartesian position or Cartesian orientation expressed using the quaternion logarithm (see Appendix A for preliminaries on unit quaternions). The DMP consists of two sets of differential equations, the transformation and the canonical system. A DMP can encode a desired trajectory t_j , $\mathbf{y}_{d,j}$ for $j = 1 \dots m$ where m is the total number of points, and through its transformation system it can generalize this trajectory spatially from an initial position \mathbf{y}_0 to a desired target position \mathbf{g} . Temporal generalization-scaling, i.e. execution of this trajectory with a different time duration or speed, is achieved through the canonical system, which provides the clock s (time substitute) for the transformation system, to avoid direct time dependency. Without loss of generality we consider a canonical system where the phase s evolves from 0 at $t = 0$ to 1 at $t = T_f$, where T_f is the desired motion duration. The transformation and canonical systems are given by [13]:

$$\ddot{\mathbf{y}} = \ddot{\mathbf{y}}_s - \mathbf{D}(\dot{\mathbf{y}} - \dot{\mathbf{y}}_s) - \mathbf{K}(\mathbf{y} - \mathbf{y}_s) \quad (1)$$

$$\ddot{s} = d(\dot{s}_d - \dot{s}), \quad s(0) = 0, \quad \dot{s}(0) = \dot{s}_d = \frac{1}{T_f} \quad (2)$$

where \mathbf{K} , $\mathbf{D} \in \mathcal{S}_{++}^n$, with \mathcal{S}_{++}^n denoting the set of symmetric $n \times n$ positive definite matrices, and \mathbf{y}_s encodes the desired

trajectory through a weighted sum of K Gaussians given by:

$$\mathbf{y}_s \triangleq \mathbf{W}^T \phi(s) \quad (3)$$

$$\dot{\mathbf{y}}_s = \mathbf{W}^T \frac{\partial \phi(s)}{\partial s} \dot{s} \quad (4)$$

$$\ddot{\mathbf{y}}_s = \mathbf{W}^T \left(\frac{\partial^2 \phi(s)}{\partial^2 s} \dot{s}^2 + \frac{\partial \phi(s)}{\partial s} \ddot{s} \right) \quad (5)$$

where $\mathbf{W} \in \mathbb{R}^{K \times n}$ are determined from $\mathbf{W} = \text{argmin}_{\mathbf{W}} J(\mathbf{W}^T \phi(s), \mathbf{y}_d)$, where J can be the Least Squares (LS), i.e. $\min_{\mathbf{W}} \sum_{j=1}^m \|\mathbf{y}_{d,j} - \mathbf{W}^T \phi_j\|_2^2$, or the Locally Weighted Regression (LWR) objective cost function [2]. The Gaussian kernels are $\phi(s)^T = [\psi_1(s) \dots \psi_N(s)] / \sum_{i=1}^K \psi_i(s)$, with $\psi_i(s) = \exp(-h_i(s - c_i)^2)$ with c_i being the centers and h_i the inverse widths. A reasonable heuristic is to set the centers c_i equally spaced in $[0, 1]$ and set $h_i = 1/(a_h(c_{i+1} - c_i))^2$ where a_h controls the standard deviation of the Gaussian kernels. Choosing $a_h \in [1.2, 1.5]$ produces empirically good approximation results.

For encoding Cartesian orientation we can simply employ the quaternion logarithm, i.e. $\mathbf{y} = \log(\mathbf{Q})$ where $\mathbf{Q} \in \mathbb{S}^3$ is the orientation as unit quaternion. We can then obtain the quaternion, rotational velocity and acceleration from \mathbf{y} and its derivatives using the mappings (15), (17) and (21) from Appendix A. Alternatively we can rewrite the transformation system as:

$$\dot{\omega} = \dot{\omega}_s - \mathbf{D}(\omega - \omega_s) - \mathbf{K} \log(\mathbf{Q} * \bar{\mathbf{Q}}_s) \quad (6)$$

where \mathbf{Q}_s , ω_s and $\dot{\omega}_s$ are obtained from (3)-(5) using (15), (17) and (21) from Appendix A.

Remark 1: Notice that in [13] we had defined $\mathbf{y}_s \triangleq \mathbf{K}_s(\mathbf{f}_p(s) - \mathbf{f}_p(0)) + \mathbf{y}_0$ with $\mathbf{f}_p(s) = \mathbf{W}^T \phi(s)$ and \mathbf{K}_s being an appropriate scaling matrix. To achieve mathematical equivalence with the original DMP [2], i.e. to generate the exact same trajectories irrespective of the existence of additional coupling terms, one has to choose $\mathbf{K}_s = \text{diag} \left(\frac{\mathbf{g} - \mathbf{y}_0}{\mathbf{f}_p(1) - \mathbf{f}_p(0)} \right)$ [13]. Other scaling matrix choices are viable like the one proposed in [3]. As we will show, this scalings can produce over-scaling of the demo trajectory resulting in large velocities and accelerations. In contrast, here we adopt a different approach for spatial generalization based on optimizing online the DMP weights \mathbf{W} so that the acceleration profile and hence the underlying pattern of the training trajectory is preserved, without producing over-scalings.

Remark 2: For Cartesian orientation in [13] we had defined $\mathbf{y} = \log(\mathbf{Q} * \bar{\mathbf{Q}}_0)$, where \mathbf{Q}_0 is the initial orientation. This was necessary when using the spatial scaling matrix \mathbf{K}_s , described in *Remark 1*, to ensure convergence to the target. However, with the proposed formulation this is no longer necessary and we can simply use directly $\mathbf{y} = \log(\mathbf{Q})$, as convergence to the target is imposed as a constraint in the proposed optimization.

III. PROPOSED GENERALIZATION

Here we present a novel generalization scheme that allows a DMP to adapt not only to new initial position \mathbf{y}_0 and

target position \mathbf{g} but also to external signals and/or via-points¹, while preserving the shape of the demonstrated trajectory. To this end, we propose to optimize the DMP weights so that the distance from the learned (from the demonstration) acceleration profile is minimized, while also satisfying the initial and final state constraints, i.e. start at $t = 0$ from \mathbf{y}_0 with zero velocity/acceleration and reach at $t = T_f$ the target \mathbf{g} , again with zero velocity/acceleration. We assume that \mathbf{g} can be time varying between 0 and T_f and is constant afterwards. To achieve this, the following optimization problem has to be solved at each time-step i :

$$\min_{\mathbf{W}} \sum_{j=1}^m \left\| \frac{\partial^2 \hat{\mathbf{y}}_{d,j}}{\partial^2 s} - \mathbf{W}^T \frac{\partial^2 \phi_j}{\partial^2 s} \right\|_2^2 \quad (7a)$$

$$\text{s.t. } \mathbf{W}^T \mathbf{A}(0) = \mathbf{Y}_0 \quad (7b)$$

$$\mathbf{W}^T \mathbf{A}(1) = \mathbf{G}_i \quad (7c)$$

$$\mathbf{W}^T \Phi_{v,i} = \mathbf{Y}_{v,i} \quad (7d)$$

$$\mathbf{W}^T \mathbf{C}_j = \mathbf{Y}_j, \quad j = 1 \dots i \quad (7e)$$

where the learned acceleration profile is $\frac{\partial^2 \hat{\mathbf{y}}_{d,j}}{\partial^2 s} = \mathbf{W}_0^T \frac{\partial^2 \phi_j}{\partial^2 s}$ with $\mathbf{W}_0 = \arg\min_{\mathbf{W}} J(\mathbf{W}^T \phi(s), \mathbf{y}_d)$ (notice from (2) that, for nominal execution, $\ddot{s} = 0$ and hence from (5) the acceleration is just $\frac{\partial^2 \hat{\mathbf{y}}_{d,j}}{\partial^2 s}$ scaled by the constant $1/T_f^2$). The matrices in the first two equality constraints, (7b), (7c), with $\mathbf{A}(s) = [\phi(s) \quad \dot{\phi}(s) \quad \ddot{\phi}(s)]$, enforce the initial state $\mathbf{Y}_0 = [\mathbf{y}_0 \quad \mathbf{0}_{n \times 1} \quad \mathbf{0}_{n \times 1}]$ and final state $\mathbf{G}_i = [\mathbf{g}_i \quad \mathbf{0}_{n \times 1} \quad \mathbf{0}_{n \times 1}]$ conditions. Via-point constraints, which can be used to locally modify a segment of the DMP trajectory, e.g. to constrain the motion in an insertion task or to push aside or avoid obstacles, are defined in (7d), where $\mathbf{Y}_{v,i} = [\mathbf{y}_{v,1} \dots \mathbf{y}_{v,L_i}]$ contains the via-points, with L_i their number at the current time-step i , and $\Phi_{v,i} = [\phi(s_{v,1}) \dots \phi(s_{v,L_i})]$.² The constraints in (7e) with $\mathbf{C}_j = \mathbf{C}(s_j) = [\phi(s_j) \quad \dot{\phi}(s_j) \quad \ddot{\phi}(s_{j-1})]$ and $\mathbf{Y}_j = [\mathbf{y}_j \quad \dot{\mathbf{y}}_j \quad \ddot{\mathbf{y}}_{j-1}]$ encode the current and all previous state constraints up to timestep i .

There are two different options for choosing \mathbf{Y}_j . The first one is to set \mathbf{Y}_j to the actual robot's state at step j so that any external signals, included as coupling terms in (1), are accounted for (in way that the preserves the demonstrated acceleration profile) in the DMP weights adaptation. This can be desirable for instance, when human contact forces intend to modify a segment of the learned DMP trajectory or when repulsive forces are added as coupling terms to avoid obstacles. Having the DMP learn online these adjustments allows the use of the final updated DMP weights in future executions of the task ensuring the following of a desired path without further adjustments. The second option is to set $\mathbf{Y}_j = \mathbf{W}_{i-1}^T \mathbf{C}_j$, preserving the previously learned trajectory, which would result in only local modulations of the output trajectory in the presence of coupling terms. This is preferable when the external signals are random non-recurring signals,

e.g. unintentional contact with a human or dynamic obstacle avoidance.

Regardless of the choice of \mathbf{Y}_j , the current state constraint for $j = i$, ensures that a smooth trajectory is generated by (1) even in the presence of abrupt target changes. The previous state constraints $\mathbf{Y}_{1:i-1}$ guarantee that if the DMP is run in reverse as in [13], using the final adapted weights from the forward execution, the same trajectory (in reverse) will be executed. This could be expedient for safely retracting after the forward execution of a task, especially if the task has geometric constraints (like an insertion) which will have to be respected in the retraction phase.

A. Online DMP weights adaptation

Solving the problem in (7) on-line at each control cycle would be too slow and hence prohibitive for real-time usage. Instead we can employ the following recursive 2-step update at each time-step $i > 0$, which has computational complexity $O(K^2)$ and can be carried out in real-time:

step 1: Remove the effect of the previous target \mathbf{g}_{i-1} and via-points:

$$\hat{\mathbf{W}}_i = \mathbf{W}_{i-1} + \hat{\mathbf{K}}_i (\hat{\mathbf{Z}}_i - \mathbf{W}_{i-1}^T \hat{\mathbf{H}}_i)^T \quad (8a)$$

$$\hat{\mathbf{P}}_i = \mathbf{P}_{i-1} - \hat{\mathbf{K}}_i \hat{\mathbf{H}}_i^T \mathbf{P}_{i-1} \quad (8b)$$

$$\hat{\mathbf{K}}_i = \mathbf{P}_{i-1} \hat{\mathbf{H}}_i (\hat{\mathbf{R}}_i + \hat{\mathbf{H}}_i^T \mathbf{P}_{i-1} \hat{\mathbf{H}}_i)^{-1} \quad (8c)$$

where

$$\hat{\mathbf{Z}}_i = [\mathbf{G}_{i-1} \quad \mathbf{Y}_{v,i}^-], \quad \hat{\mathbf{H}}_i = [\mathbf{A}(1) \quad \Phi_{v,i}^-], \quad \hat{\mathbf{R}}_i = -\epsilon \mathbf{I}_{3+b_i^-} \quad (9)$$

with $\epsilon \approx 0^+$ and $\mathbf{Y}_{v,i}^- \in \mathbb{R}^{n \times b_i^-}$ containing in columns the via-points that exist in the columns of $\mathbf{Y}_{v,i-1}$ and not in $\mathbf{Y}_{v,i}$ (i.e. are present at time-step $i-1$ and not at i)³ and $\Phi_{v,i}^- = [\phi(s_k)]_{k=1:b_i^-}$ with s_k being the phase corresponding to each via-point in $\mathbf{Y}_{v,i}^-$.

step 2: Update to new target-constraints:

$$\mathbf{W}_i = \hat{\mathbf{W}}_i + \mathbf{K}_i (\mathbf{Z}_i - \hat{\mathbf{W}}_i^T \mathbf{H}_i)^T \quad (10a)$$

$$\mathbf{P}_i = \hat{\mathbf{P}}_i - \mathbf{K}_i \mathbf{H}_i^T \hat{\mathbf{P}}_i \quad (10b)$$

$$\mathbf{K}_i = \hat{\mathbf{P}}_i \mathbf{H}_i (\mathbf{R}_i + \mathbf{H}_i^T \hat{\mathbf{P}}_i \mathbf{H}_i)^{-1} \quad (10c)$$

where

$$\mathbf{Z}_i = [\mathbf{Y}_i \quad \mathbf{G}_i \quad \mathbf{Y}_{v,i}^+], \quad \mathbf{H}_i = [\mathbf{C}_i \quad \mathbf{A}(1) \quad \Phi_{v,i}^+], \quad \mathbf{R}_i = \epsilon \mathbf{I}_{6+b_i^+} \quad (11)$$

with $\mathbf{Y}_{v,i}^+ \in \mathbb{R}^{n \times b_i^+}$ containing in columns the via-points that are present at time-step i and not at $i-1$ and $\Phi_{v,i}^+ = [\phi(s_k)]_{k=1:b_i^+}$ with s_k being the phase corresponding to each via-point in $\mathbf{Y}_{v,i}^+$.

For initialization at step $i = 0$ we set $\mathbf{Z}_0 = [\mathbf{Y}_0 \quad \mathbf{G}_0]$, $\mathbf{H}_0 = [\mathbf{A}(0) \quad \mathbf{A}(1)]$, $\mathbf{R}_0 = \epsilon \mathbf{I}_6$, $\hat{\mathbf{W}}_0 = \mathbf{W}_0$ and $\hat{\mathbf{P}}_0 = \mathbf{P}_0$ where

$$\mathbf{W}_0 = \arg\min_{\mathbf{W}} J(\mathbf{W}^T \phi(x), \mathbf{y}_d), \quad \mathbf{P}_0 = \left(\sum_{j=1}^m \frac{\partial^2 \phi_j}{\partial^2 s} \frac{\partial^2 \phi_j}{\partial^2 s}^T \right)^{-1}$$

¹The term "point" can refer either to joint positions, Cartesian position, Cartesian orientation or Cartesian pose.

²If the phase $s_{v,l}$, $l = 1 \dots L_i$, is not provided explicitly, a reasonable heuristic is to calculate it as $s_v = \arg\min_{s_k} \|\mathbf{y}_s(s_k) - \mathbf{y}_v\|$, where s_k in uniformly sampled in $(s, 1]$. Empirically, taking approximately 80 samples is sufficient, as the minimization need not be exact.

³Such is the case for instance if they are defined relative to a varying target or an object, whose position has changed or has been completely removed.

Remark 3: At the beginning of each execution, the DMP weights are initialized to the values that have been calculated offline once during the DMP training from the demonstration. Alternatively, if at a previous execution the DMP was adjusted to some external signals, resulting to some final weights \mathbf{W}_f , and it is desirable to retain this adjusted pattern at subsequent executions, one could set $\mathbf{W}_0 = \mathbf{W}_f$.

Remark 4: When \mathbf{g} is constant and/or we don't wish to adapt the DMP trajectory to external signals or via-points, we can drop the constraints in (7d), (7e). It suffices to carry the above update only once at the beginning with \mathbf{Z}_0 , \mathbf{H}_0 and \mathbf{R}_0 to obtain \mathbf{W}_1 and use $\mathbf{W}_i = \mathbf{W}_1$ for $i > 1$.

Remark 5: In practice, due to finite numerical precision, setting ϵ in $\hat{\mathbf{R}}_i$, \mathbf{R}_i very close to zero can make the matrix being inverted in (8c) and (10c) ill-conditioned. We have found that in practice choosing ϵ approximately in the range $(10^{-10}, 10^{-6})$ does not create any numerical issues and the constraints are satisfied within an error tolerance of the order of 10^{-4} or even less depending on how small ϵ is.

Remark 6: Despite using the same value ϵ in the above analysis for simplicity, it is easy to verify that different values of ϵ can be chosen for each type of constraint. The selected ϵ value can facilitate finding a solution in the optimization problem (7) in case constraints cannot be strictly satisfied (i.e. infinite accuracy). Then, the value of ϵ essentially relaxes equality constraints, by penalizing the cost function (see *Theorem 3* from Appendix B). Choosing different values of ϵ for each type of constraint, allows to prioritize which of these constraints should be satisfied with greater accuracy. Moreover, when adapting to external signals which contain noise, higher values of ϵ can be used to suppress that noise.

B. Derivation/Proof of the weights adaptation

In the following, we prove that (8), (10) solve the initial optimization problem given in (7). To this end, we will utilize the theorems provided in Appendix B. Problem (7) can be written compactly as:

$$\begin{aligned} \min_{\mathbf{W}} \text{tr}\{(\ddot{\mathbf{Y}}_d - \mathbf{W}^T \ddot{\mathbf{\Phi}})^T (\ddot{\mathbf{Y}}_d - \mathbf{W}^T \ddot{\mathbf{\Phi}})\} \\ \text{s.t. } \mathbf{W}^T \bar{\mathbf{H}}_i = \bar{\mathbf{Z}}_i \end{aligned} \quad (12)$$

where $\ddot{\mathbf{Y}}_d = [\frac{\partial^2 \mathbf{y}_{d,1}}{\partial^2 s} \dots \frac{\partial^2 \mathbf{y}_{d,m}}{\partial^2 s}] \in \mathbb{R}^{n \times m}$, $\ddot{\mathbf{\Phi}} = [\frac{\partial^2 \phi_1}{\partial^2 s} \dots \frac{\partial^2 \phi_m}{\partial^2 s}] \in \mathbb{R}^{K \times m}$, $\bar{\mathbf{Z}}_i = [\mathbf{Y}_0 \quad \mathbf{G}_i \quad \mathbf{Y}_{1:i} \quad \mathbf{Y}_{v,i}] \in \mathbb{R}^{n \times m_1}$ and $\bar{\mathbf{H}}_i = [\mathbf{A}(0) \quad \mathbf{A}(1) \quad \mathbf{C}_{1:i} \quad \mathbf{\Phi}_{v,i}] \in \mathbb{R}^{K \times m_1}$ with $m_1 = 6 + 3i + \bar{L}_i$. Based on *Theorem 4* problem (12) is equivalent to:

$$\begin{aligned} \min_{\mathbf{W}} f_i(\mathbf{W}) \triangleq \text{tr}\{(\ddot{\mathbf{Y}}_d - \mathbf{W}^T \ddot{\mathbf{\Phi}})^T (\ddot{\mathbf{Y}}_d - \mathbf{W}^T \ddot{\mathbf{\Phi}})\} \\ + \text{tr}\{(\bar{\mathbf{Z}}_i - \mathbf{W}^T \bar{\mathbf{H}}_i)^T \bar{\mathbf{R}}_i^{-1} (\bar{\mathbf{Z}}_i - \mathbf{W}^T \bar{\mathbf{H}}_i)\} \end{aligned} \quad (13)$$

for $\bar{\mathbf{R}}_i = \epsilon \mathbf{I}_{m_1}$, $\epsilon \approx 0^+$. Given now the solution at timestep $i-1$ for problem (13) we want to find the solution for timestep i , for which the cost function can be written as:

$$f_i = \hat{f}_{i-1} + \text{tr}\{(\mathbf{Z}_i - \mathbf{W}^T \mathbf{H}_i)^T \mathbf{R}_i^{-1} (\mathbf{Z}_i - \mathbf{W}^T \mathbf{H}_i)\}$$

where $\hat{f}_{i-1} = f_{i-1} - \text{tr}\{(\hat{\mathbf{Z}}_i - \mathbf{W}^T \hat{\mathbf{H}}_i)^T \hat{\mathbf{R}}_i^{-1} (\hat{\mathbf{Z}}_i - \mathbf{W}^T \hat{\mathbf{H}}_i)\}$. Invoking *Theorem 5* the solution to \hat{f}_{i-1} is given by (8).

Using now *Theorem 3* the solution to f_i is equivalent to the solution of $\text{tr}\{(\mathbf{W} - \hat{\mathbf{W}}_i)^T \hat{\mathbf{P}}_i (\mathbf{W} - \hat{\mathbf{W}}_i)\} + \text{tr}\{(\mathbf{Z}_i - \mathbf{W}^T \mathbf{H}_i)^T \mathbf{R}_i^{-1} (\mathbf{Z}_i - \mathbf{W}^T \mathbf{H}_i)\}$, which based on *Theorem 2* is given by (10).

IV. SIMULATIONS

In the following we compare the DMP produced with the proposed generalization, henceforth referred as DMP⁺⁺, with the classical DMP, as well as other variations that have been proposed in the literature. We further demonstrate and comment on the effects of adaptation to external signals, via-points and also including kinematic limits (inequality constraints) using the proposed generalization with [14]. Unless stated otherwise, in all cases, based on *Remark 6* and in the spirit that higher priority should be placed on the initial and final position constraints followed by the via-point constraints and then the previous state constraints, we chose $\epsilon 10^{-9}$ for the initial and final position, 10^{-7} for the initial and final velocity and acceleration constraints, 10^{-7} for via-points and 10^{-6} , 10^{-4} , for the previous state constraint. Notice that violation of the previous state constraint generates a discontinuous acceleration in the DMP (1), which will be larger the bigger the error in the equality constraint is.

A. Spatial generalization comparison

We start off by examining the three basic cases where the classical DMP scaling is problematic [4]. For simplicity we consider an 1 DoF demonstration starting at position zero. Simulation results for each case are plotted in Fig. 1, where the demo is plotted with green dashed line, the proposed DMP⁺⁺ with blue and the classical DMP with magenta dotted line. In the first case (Fig. 1a) the demonstrated target \mathbf{g}_d is quite close to the initial position $\mathbf{y}_{0,d} = 0$. In this case, even a new target that is close to that of the demo, results in over-scaling for the classical DMP. In the figure, the resulting trajectory for the classical DMP is scaled by 400 for visualization purposes (the position actually converges to \mathbf{g} but in the plot due to the scaling by 400 it is $\mathbf{g}/400 \approx 0$). In the second case (Fig. 1b) the demo initial and target positions are different but the new target is the same with the initial position i.e. $\mathbf{g} = \mathbf{y}_0$. In this case, no motion is generated by the classical DMP. Finally, in the third case (Fig. 1c), if the new target is chosen below the initial position, or more generally when $\text{sign}(\mathbf{g} - \mathbf{y}_0) = -\text{sign}(\mathbf{g}_d - \mathbf{y}_{0,d})$, the classical DMP produces a mirrored trajectory. Unlike the classical DMP, the proposed DMP⁺⁺ retains the shape of the demonstrated trajectory in all cases, without exhibiting any side-effects.

We further compare our method with the scaling proposed in [3], which we will call DMP-rot, and the so called bio-inspired DMP variation from [4], referred here as DMP-bio. Simulations were conducted, using as demo a Cartesian position trajectory depicted with green dashed line in Fig. 2. Notice that the demonstrated initial position \mathbf{p}_0 (green circle) and target position \mathbf{g}_d (light red cross) are not close. Despite that, the generated trajectory to the new target \mathbf{g} (vivid red cross) still produces a large scaling for DMP-rot (cyan dash-dotted line), which is attributed to the fact that all DoFs are

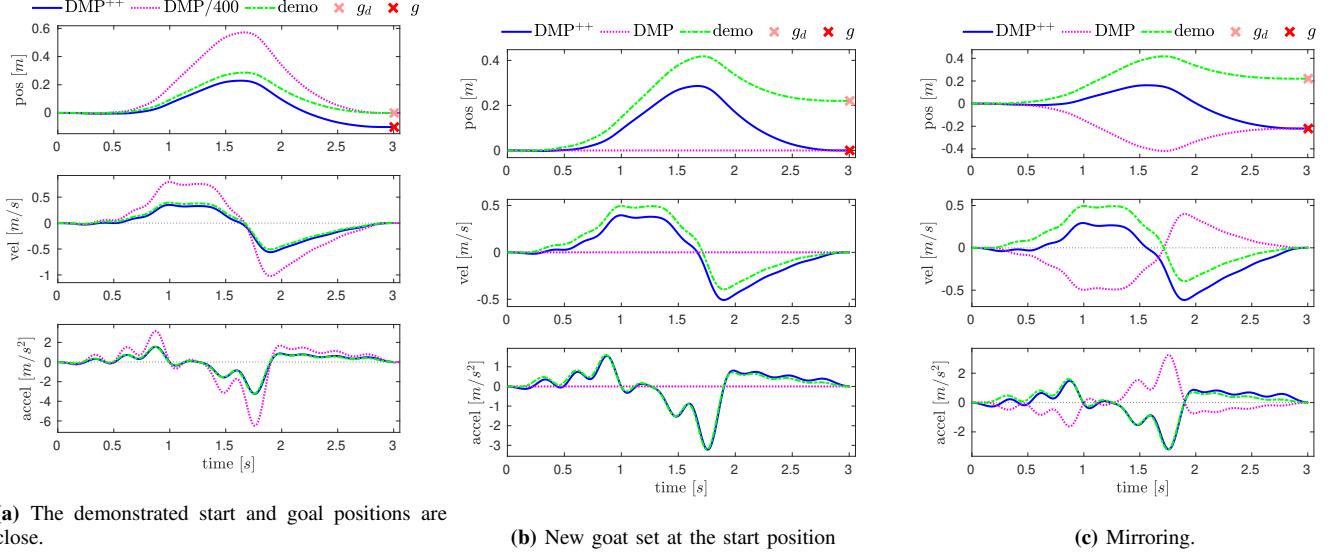


Fig. 1: Comparison with classical DMP generalization.

scaled by $\|g - y_0\|$, therefore even though the offset along the z -axis is moderate, the offset of g by 1 m in the xy -plane increases the overall scaling. DMP-bio (light brown line) does not result in over-scaling, however the amplitude of the trajectory is shifted, distorting slightly the demonstrated shape. This is attributed to the fact that DMP-bio tracks a time-varying attractor that shifts exponentially from tracking the demo w.r.t. the initial position to tracking it w.r.t. the new target (this can be verified by analyzing the forcing term in [4], analogous to the analysis in [13]). The result is a drag/shift of the trajectory that gets more pronounced the further the new target is from the demonstrated one. On the other hand, the proposed DMP++ (blue line) does not exhibit any of the aforementioned drawbacks.

B. Generalization to target perturbations

We further test out method in a scenario where the target position changes abruptly at discrete time-steps and compare it to using the classical DMP with goal-filtering [2], i.e. the DMP target is updated as $\dot{g} = a_g(g_{\text{new}} - g)$. The results are plotted in Fig. 3, where the target is shown with red. Both the proposed DMP++ (blue line) and the DMP with goal filtering (magenta dashed line) produce continuous trajectories and converge to the target. Nevertheless, the DMP with goal filtering generates higher accelerations at the time-instants the target changes, even though the filtering constant is selected at a value $a_g = 4$ that yields a slow settling time of about 200 ms.

C. Adaptation to external signals

To demonstrate the ability of our method to adapt and generalize to external signals and at the same time retain as much as possible the shape of the demonstration, we consider an obstacle avoidance scenario, where the external signals are the repulsive forces generated by a repulsive artificial potential associated with each obstacle, activated along an offset d_0 from it as defined in [15]. The method is presented in [15] for obstacle modeled by spheres but it can be generalized for any other analytic smooth surface like an ellipsoid or a plane which we use in this simulation. In particular, denoting by $\mathcal{O} = \{y \in \mathbb{R}^n : \psi_o(y) = 0\}$ the surface of an obstacle, for an ellipsoid we have $\psi_o(y) = (y - c)^T \Sigma^{-1} (y - c) - 1$, where c is the center and Σ the covariance, and for a plane $\psi_o(y) = n^T (y - y_0)$, where n is the vector normal to the plane and y_0 any point on the surface plane. By defining the normalized distance $e = \frac{(\psi_o(y) - d_0)^2}{d_0^2}$ if $\psi_o(y) \leq d_0$, otherwise $e = 0$ and the barrier potential $V_o = -\log(1 - e)$ which is zero for $\psi_o(y) \geq d_0$ and tends to $+\infty$ on the surface i.e. as $\psi_o(y) \rightarrow 0$, a valid repulsive force that prevents the penetration of the surface can be obtained as $f_{\text{rep}} = -k_o \frac{\partial V_o}{\partial y}$, where $k_o > 0$ controls the magnitude of the repulsive force.

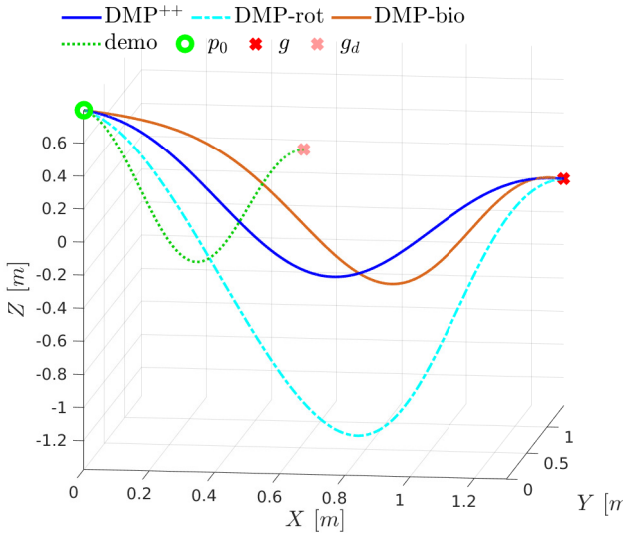


Fig. 2: Generalization comparison between the proposed and other DMP variants.

respect kinematic limits like position velocity and acceleration bounds as well as passing from via-points. We show that by modifying the framework from [14] according to Fig. 5, where the DMP with the classical scaling is replaced by DMP⁺⁺ we achieve more efficient generalization that accounts also for via-points and external signals. Notice that via-points are included both in DMP⁺⁺ and in the optimization module of [14] (Fig. 5 brown rectangle) via the respective equality constraints so as to guarantee that the constrained within the kinematic inequality limits trajectory will also pass from the via-points.

Simulation results of a 1 DoF example with two via points and position, velocity and acceleration limits are shown in Fig. 6, where the method proposed in [14] is used to optimize the velocity profile with all relevant parameters chosen as in [14]. To endow the optimizer with greater flexibility in finding feasible solutions we consider the kinematic limits as hard limits (grey dashed lines) and introduce the lower and upper soft limits (magenta dashed lines) within the hard limits. We want to preferably operate within the soft limits and only exceed them if feasibility would be inevitable otherwise [14]. It can be observed that the DMP⁺⁺ (blue line) retains the shape of the demonstration (green dash dotted line), even in the presence of kinematic limits and via-points (red asterisks). On the other hand, the DMP with the classical scaling (mustard dotted line) can induce large scalings that generate velocities and accelerations that violate considerably the limits, leading to saturation (see the 2nd and 3rd subplots of Fig. 6) and consequently the distortion of the demonstrated shape, as can be observed comparing the mustard with the green trajectory in the first subplot. This distortion would be even more adverse for cases in which scaling is problematic like those presented in Fig. 1, where a feasible solution may even not be found.

V. EXPERIMENTAL RESULTS

To validate experimentally our method we consider a scenario where a robot has to pick a carton from a conveyor belt and insert it inside a box. The pose of the carton and the box are tracked using apriltags with a frame rate of 30 Hz. Two DMP are trained through PbD, one for picking and the second for inserting the carton in the box. We examined the two scenarios depicted in Fig. 7. In the first (top picture), the carton is moving on the conveyor belt and a perturbation of its pose is also introduced by having a human displace it during execution. In the second scenario (bottom picture), an obstacle obstructs the robot from picking the carton. In this scenario two variants are examined: a) introducing a coupling term from a force exerted by a human, who intervenes to guide the robot over the obstacle or b) using via-points, obtained from an apriltag that the human uses to demonstrate a detour around the obstacle.

In all experiments, to guarantee that the carton is properly inserted in the box, we specified 5 additional via-points with the same orientation with the carton's target with 3 cm offset between them starting from the target position. Moreover, to further highlight the robustness of our method, in all experiments during the placing of the carton, the target pose of the box (and hence its associated via-points) are altered on the fly.

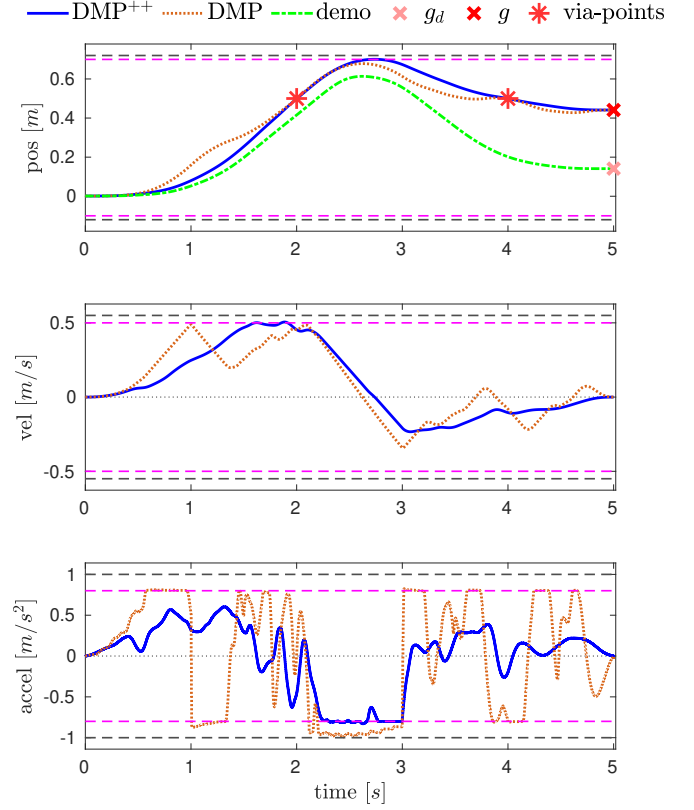


Fig. 6: Comparison of the classical DMP generalization against the proposed DMP⁺⁺ in combination with [14] to enforce kinematic inequality constraints.

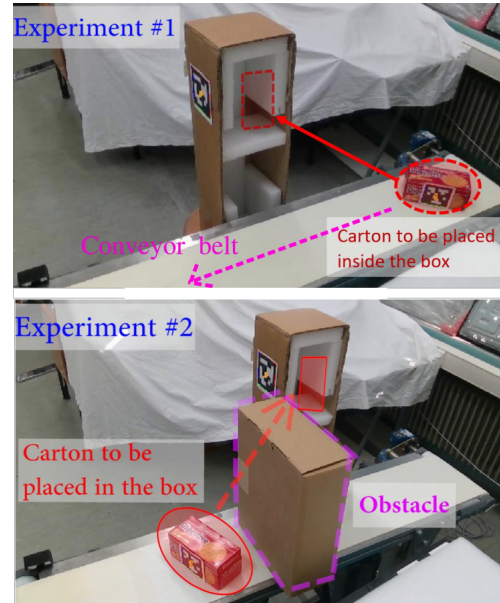


Fig. 7: Experimental setup.

To carry out these experiments a velocity controlled ur5e robot is used, with 2 ms control cycle, which takes as reference the velocity produced by the DMP transformation system from (1), where \mathbf{y} is either the Cartesian position or for orientation

$\mathbf{y} = \log(\mathbf{Q} * \bar{\mathbf{Q}}_0)$. We also add in (1) the coupling term $\mathbf{u} = \mathbf{J}_i \mathbf{M}_i^{-1} \mathbf{f}_i - a_i \ddot{\mathbf{y}}_s$, where $i \in \{p, o\}$ for position and orientation respectively, $\mathbf{J}_p = \mathbf{I}_3$, $\mathbf{J}_o = \mathbf{J}_\eta^T$ (see (25)), $\mathbf{M}_p = 5$ and $\mathbf{M}_o = 2$ can be interpreted as the desired inertia in (1), with damping $\mathbf{M}_i \mathbf{D}$ and stiffness $\mathbf{M}_i \mathbf{K}$, \mathbf{f}_i is the external force/torque measured by the robot's F/T sensor at its wrist and $a_i \ddot{\mathbf{y}}_s$, with $a_i = \sqrt{\min(2 \|\mathbf{f}_i\|, 1.0)}$, is used to mitigate the effect of the feed-forward acceleration $\ddot{\mathbf{y}}_s$ of the DMP whenever the external force/torque is greater than 0.5 N/Nm. This is useful when there is undesired contact or when the human guides physically the robot to alter its trajectory. The DMP weights are updated online according to (8), (10), while ϵ was set as in the simulations. The current state constraint in the optimization is set to the actual robot's state. In all cases, the optimization at each control cycle was below 0.8 ms, which is well within the 2ms control cycle of the robot. For the canonical system from (2), we define $\dot{s}_d = \dot{s}_1 / (1 + a_d \|\mathbf{f}_p\|)$, $a_d > 0$, which is used to enable phase stopping when an external force is applied. For forward execution we set $s(0) = 0$ and $\dot{s}(0) = \dot{s}_1 = \frac{1}{T_f}$, while for reverse (retraction) $s(0) = 1$ and $\dot{s}(0) = \dot{s}_1 = -\frac{1}{T_f}$. Also, for the case that we want the DMP to adapt to external signals (experiment 2 - case (b)) we disable phase stopping, i.e. $\dot{s}_d = \dot{s}_1$, as in this case the measured external force is used to adapt the DMP trajectory and is not meant to stop its evolution.

A video with the complete experimental scenarios along with extensive explanations and visualizations can be found at dropbox.com/s/9vfgs2qc8bwsbvt/video.mp4. Indicative results from scenario 1 (Fig. 7, top picture) are plotted in Fig. 8. On the top subplot, it can be observed that continuous changes or even abrupt changes of the target during pick (red line) and place (magenta) are handled smoothly by the proposed DMP (blue and cyan line). On the bottom subplot, the phase variable evolution is plotted, where during placing at $t \approx 12$ sec, the human holds the robot's end-effector and the exerted force (mustard line) triggers phase stopping, while in the meantime the human displaces the box (top plot, magenta line).

For the second scenario, the results in Fig. 9 demonstrate on the top the adjusted DMP trajectory during the pick (brown line) along the x -axis, where the maximal deviation from the nominal trajectory (magenta dashed line) occurred. This adaptation required a moderate human force (mustard line) of less than 6 N. On the bottom subplot, the paths for the pick and place are drawn, where for the place the associated via-points are also visualized, from the initial to the finally displaced position of the box. Finally, the same scenario is revisited, only this time the human does not interact physically with the robot. Instead, he uses an apriltag as indicator of the via-points' pose, through which the robot should pass. Results are presented in Fig. 10. where on top, the via-points and the DMP adjusted trajectory along the x -axis is plotted, and on the bottom, the 3D paths and the via-points are visualized.

VI. CONCLUSIONS

In this work we presented a novel generalization scheme for DMP, based on optimizing online the DMP weights, so as

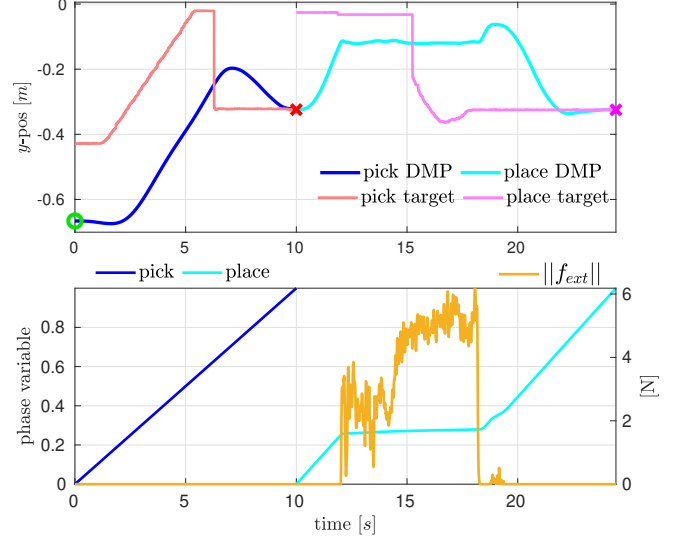


Fig. 8: Experiment 1. Top: y position of the DMP (blue line) for picking the carton (red line) and the DMP (cyan line) for placing the carton in the box (magenta line). Bottom: Phase variable evolution for picking (blue) and for placing (cyan) superimposed with the external force (mustard line).

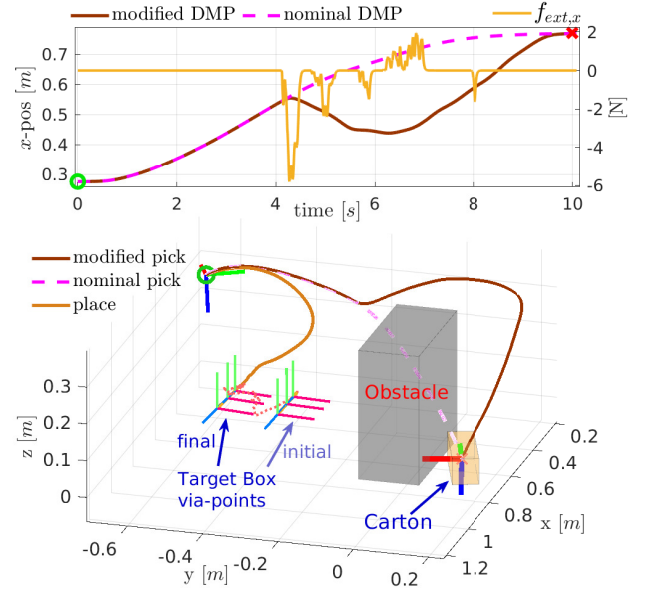


Fig. 9: Experiment 2-case a: Adaptation of DMP to external force. Top: x -position of nominal (dashed magenta line) and the modified DMP (brown line) for picking the carton, superimposed with the applied force (mustard line). Bottom: Cartesian path of the DMP for picking and placing the carton in the box.

to preserve the demonstrated trajectory shape. The proposed generalization has been shown to achieve efficient generalization even in cases where the classical DMP generalization was problematic. Moreover, we demonstrated how this method can extend the online adaptation and generalization properties of DMP, through the incorporation of via-points and external signals. All the aforementioned properties were extensively validated through simulations and experiments.

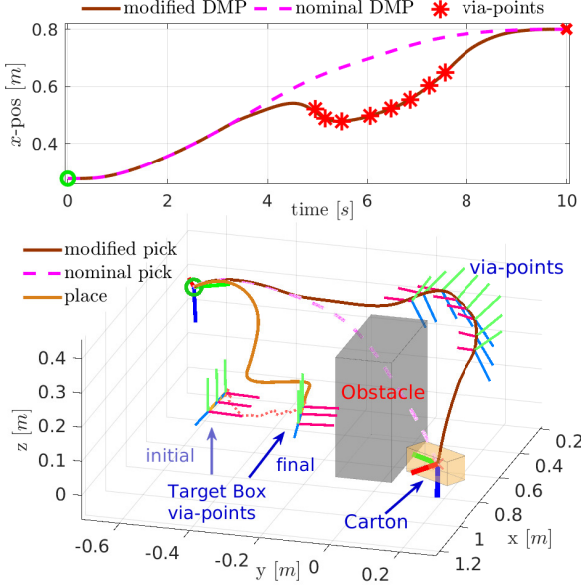


Fig. 10: Experiment 2-case b: Adaptation of DMP with via-points. Top: x -position of nominal (dashed magenta line) and the modified DMP (brown line) for picking the carton. Bottom: Cartesian path of the DMP for picking and placing the carton in the box.

APPENDIX A - UNIT QUATERNION PRELIMINARIES

Given a rotation matrix $\mathbf{R} \in SO(3)$, an orientation can be expressed in terms of the unit quaternion $\mathbf{Q} \in \mathbb{S}^3$ as $\mathbf{Q} = [w \ \mathbf{v}^T]^T = [\cos(\theta_2) \ \sin(\theta_2)\mathbf{k}^T]^T$, where $\mathbf{k} \in \mathbb{S}^2$, $\theta_2 = \theta/2$ with $\theta \in [-\pi, \pi)$ are the equivalent unit axis-angle representation. The quaternion product between the unit quaternions $\mathbf{Q}_1, \mathbf{Q}_2$ is denoted as $\mathbf{Q}_1 * \mathbf{Q}_2$. The inverse of a unit quaternion is equal to its conjugate which is $\mathbf{Q}^{-1} = \mathbf{Q} = [w \ -\mathbf{v}^T]^T$. The logarithmic $\boldsymbol{\eta} = \log(\mathbf{Q})$ and exponential $\mathbf{Q} = \exp(\boldsymbol{\eta})$ mappings $\log : \mathbb{S}^3 \rightarrow \mathbb{R}^3$, $\exp : \mathbb{R}^3 \rightarrow \mathbb{S}^3$ respect the manifold's geometry and are defined as follows:

$$\log(\mathbf{Q}) \triangleq \begin{cases} 2 \cos^{-1}(w) \frac{\mathbf{v}}{\|\mathbf{v}\|}, & |w| \neq 1 \\ [0, 0, 0]^T, & \text{otherwise} \end{cases} \quad (14)$$

$$\exp(\boldsymbol{\eta}) \triangleq \begin{cases} [\cos(\|\boldsymbol{\eta}/2\|), \sin(\|\boldsymbol{\eta}/2\|) \frac{\boldsymbol{\eta}^T}{\|\boldsymbol{\eta}\|}]^T, & \|\boldsymbol{\eta}\| \neq 0 \\ [1, 0, 0, 0]^T, & \text{otherwise} \end{cases} \quad (15)$$

It can be found analytically that the relations between the rotational velocity and the derivative of the quaternion logarithm are:

$$\boldsymbol{\omega} = \mathbf{J}_\eta \dot{\boldsymbol{\eta}} \quad (16)$$

$$\dot{\boldsymbol{\eta}} = \mathbf{J}_\eta^\dagger \boldsymbol{\omega} \quad (17)$$

where

$$\mathbf{J}_\eta \triangleq \mathbf{k}\mathbf{k}^T + \frac{\sin(\theta_2) \cos(\theta_2)}{\theta_2} (\mathbf{I}_3 - \mathbf{k}\mathbf{k}^T) + \frac{\sin^2(\theta_2)}{\theta_2} [\mathbf{k}]_\times \quad (18)$$

$$\mathbf{J}_\eta^\dagger = \mathbf{k}\mathbf{k}^T + \frac{\theta_2 \cos(\theta_2)}{\sin(\theta_2)} (\mathbf{I}_3 - \mathbf{k}\mathbf{k}^T) - \theta_2 [\mathbf{k}]_\times \quad (19)$$

where $[\mathbf{k}]_{\text{times}}$ denotes the skew-symmetric matrix of \mathbf{k} . For $\theta = 0$ it can be easily verified that taking the limit of (18), (19) and using L'Hospital's rule we get $\mathbf{J}_\eta = \mathbf{J}_\eta^\dagger = \mathbf{I}_3$.

Differentiating (16), (17) we can obtain the relations between the quaternion logarithm second time derivative and the rotational acceleration:

$$\dot{\boldsymbol{\omega}} = \mathbf{J}_\eta \ddot{\boldsymbol{\eta}} + \dot{\mathbf{J}}_\eta \dot{\boldsymbol{\eta}} \quad (20)$$

$$\ddot{\boldsymbol{\eta}} = \mathbf{J}_\eta^\dagger \dot{\boldsymbol{\omega}} + \dot{\mathbf{J}}_\eta^\dagger \boldsymbol{\omega} \quad (21)$$

where

$$\begin{aligned} \dot{\mathbf{J}}_\eta = & \left(1 - \frac{\sin(\theta_2) \cos(\theta_2)}{\theta_2}\right) (\dot{\mathbf{k}}\mathbf{k}^T + \mathbf{k}\dot{\mathbf{k}}^T) + \frac{\sin^2(\theta_2)}{\theta_2} [\dot{\mathbf{k}}]_\times \\ & + \left(\frac{1 - 2\sin^2(\theta_2)}{\theta_2} - \frac{\sin(\theta_2) \cos(\theta_2)}{\theta_2^2}\right) \dot{\theta}_2 (\mathbf{I}_3 - \mathbf{k}\mathbf{k}^T) \\ & + \left(\frac{2\sin(\theta_2) \cos(\theta_2)}{\theta_2} - \frac{\sin^2(\theta)}{\theta_2^2}\right) \dot{\theta}_2 [\mathbf{k}]_\times \end{aligned} \quad (22)$$

$$\begin{aligned} \dot{\mathbf{J}}_\eta^\dagger = & \left(1 - \frac{\theta_2 \cos(\theta_2)}{\sin(\theta_2)}\right) (\dot{\mathbf{k}}\mathbf{k}^T + \mathbf{k}\dot{\mathbf{k}}^T) - \dot{\theta}_2 [\mathbf{k}]_\times - \theta_2 [\dot{\mathbf{k}}]_\times \\ & + \left(\frac{\sin(\theta_2) \cos(\theta_2) - \theta_2}{\sin^2(\theta_2)}\right) \dot{\theta}_2 (\mathbf{I}_3 - \mathbf{k}\mathbf{k}^T) \end{aligned} \quad (23)$$

with $\dot{\theta}_2 = \frac{1}{2} \mathbf{k}^T \dot{\boldsymbol{\eta}}$ and $\dot{\mathbf{k}} = \frac{1}{2} \left(\frac{1 - \mathbf{k}\mathbf{k}^T}{\theta_2} \dot{\boldsymbol{\eta}} \right)$. Taking the limit of (22), (23) for $\theta = 0$ we have that $\dot{\mathbf{J}}_\eta = \dot{\mathbf{J}}_\eta^\dagger = \mathbf{0}$.

Finally, the relations between the Cartesian torque $\boldsymbol{\tau}$ and its transformation in the quaternion logarithm space $\boldsymbol{\tau}_\eta$ is given by:

$$\boldsymbol{\tau}_\eta = \mathbf{J}_\eta^T \boldsymbol{\tau} \quad (24)$$

$$\boldsymbol{\tau} = (\mathbf{J}_\eta^\dagger)^T \boldsymbol{\tau}_\eta \quad (25)$$

These mappings follow readily from the preservation of power, i.e. it should hold that $\boldsymbol{\omega}^T \boldsymbol{\tau} = \dot{\boldsymbol{\eta}}^T \boldsymbol{\tau}_\eta$.

APPENDIX B - RECURSIVE LEAST SQUARES DERIVATIONS

Here we provide some useful results in the form of theorems which facilitate the proof of the update formulas (8), (10) that solve (7). Results in Section 2 from [16] for vectors are here extended for matrices in *Theorems 1, 2* and 5. *Theorems 1, 2* are used in the proof of *Theorems 3 – 5*, and *Theorems 2 – 5* are employed in the proof for solving (7).

Theorem 1: The solution to the problem:

$$\min_{\mathbf{W}} \text{tr}\{(\mathbf{Y} - \mathbf{W}^T \boldsymbol{\Phi})^T \mathbf{R}^{-1} (\mathbf{Y} - \mathbf{W}^T \boldsymbol{\Phi})\} \quad (26)$$

with $\mathbf{Y} \in \mathbb{R}^{n \times m}$, $\mathbf{W} \in \mathbb{R}^{k \times n}$, $\boldsymbol{\Phi} \in \mathbb{R}^{k \times m}$, $\text{rank}(\boldsymbol{\Phi}) = k$, $\mathbf{R} \in \mathcal{S}_{++}^n$ is given by:

$$\mathbf{W}_0 = \mathbf{P}_0 \boldsymbol{\Phi} \mathbf{R}^{-1} \mathbf{Y}^T \quad (27)$$

$$\mathbf{P}_0 = (\boldsymbol{\Phi} \mathbf{R}^{-1} \boldsymbol{\Phi}^T)^{-1} \quad (28)$$

where $\mathbf{P}_0 > \mathbf{0}$.

Proof: Taking the derivative of f_0 w.r.t. \mathbf{W} and solving for \mathbf{W} , it is straightforward to verify that the solution is indeed given by \mathbf{W}_0 , where $\mathbf{P} > \mathbf{0}$ since $\mathbf{R} > \mathbf{0}$ and $\text{rank}(\boldsymbol{\Phi}) = k$. ■

Theorem 2: The solution to the problem:

$$\min_{\mathbf{W}} f_0(\mathbf{W}) + \text{tr}\{(\mathbf{Z} - \mathbf{W}^T \mathbf{H})^T \mathbf{R}_1^{-1} (\mathbf{Z} - \mathbf{W}^T \mathbf{H})\} \quad (29)$$

with $f_0(\mathbf{W}) = \text{tr}\{(\mathbf{Y} - \mathbf{W}^T \bar{\Phi})^T \mathbf{R}^{-1}(\mathbf{Y} - \mathbf{W}^T \bar{\Phi})\}$, $\mathbf{Y} \in \mathbb{R}^{n \times m}$, $\mathbf{W} \in \mathbb{R}^{k \times n}$, $\bar{\Phi} \in \mathbb{R}^{k \times m}$, $\text{rank}(\bar{\Phi}) = k$, $\mathbf{R}, \mathbf{R}_1 \in \mathcal{S}_{++}^n$, $\mathbf{Z} \in \mathbb{R}^{n \times l}$, $\mathbf{H} \in \mathbb{R}^{k \times l}$, can be obtained from the solution \mathbf{W}_0 , \mathbf{P}_0 of $\min_{\mathbf{W}} f_0(\mathbf{W})$ as follows:

$$\mathbf{W}_1 = \mathbf{W}_0 + \mathbf{P}_0 \mathbf{H} (\mathbf{R}_1 + \mathbf{H}^T \mathbf{P}_0 \mathbf{H})^{-1} (\mathbf{Z} - \mathbf{W}_0^T \mathbf{H})^T \quad (30)$$

$$\mathbf{P}_1 = \mathbf{P}_0 - \mathbf{P}_0 \mathbf{H} (\mathbf{R}_1 + \mathbf{H}^T \mathbf{P}_0 \mathbf{H})^{-1} \mathbf{H}^T \mathbf{P}_0 \quad (31)$$

$$\mathbf{P}_1^{-1} = \mathbf{P}_0 + \mathbf{H} \mathbf{R}_1^{-1} \mathbf{H}^T \quad (32)$$

where $\mathbf{P}_1 > \mathbf{0}$.

Proof: We can rewrite the cost function in (29) as

$$\text{tr}\{(\bar{\mathbf{Y}} - \mathbf{W}^T \bar{\Phi})^T \bar{\mathbf{R}}^{-1}(\bar{\mathbf{Y}} - \mathbf{W}^T \bar{\Phi})\}$$

with

$$\bar{\mathbf{Y}} = [\mathbf{Y}^T \ \mathbf{Z}^T]^T, \ \bar{\Phi} = [\Phi^T \ \mathbf{H}^T]^T, \ \bar{\mathbf{R}} = \text{blkdiag}(\mathbf{R}, \mathbf{R}_1)$$

and apply the result of *Theorem 1* to get:

$$\mathbf{W} = \mathbf{P}_1^{-1} \bar{\Phi} \bar{\mathbf{R}}^{-1} \bar{\mathbf{Y}}^T = \mathbf{P}_1^{-1} (\Phi \mathbf{R}^{-1} \mathbf{Y}^T + \mathbf{H} \mathbf{R}_1^{-1} \mathbf{Z}^T) \quad (33)$$

where $\mathbf{P}_1^{-1} = \bar{\Phi} \bar{\mathbf{R}}^{-1} \bar{\Phi}^T = (\mathbf{P}_0^{-1} + \mathbf{H} \mathbf{R}_1^{-1} \mathbf{H}^T)$ with $\mathbf{P}_0^{-1} = \Phi \mathbf{R}^{-1} \Phi^T$. It follows that $\mathbf{P}_1^{-1} > \mathbf{0}$, since $\mathbf{P}_0^{-1} > \mathbf{0}$, due to $\mathbf{R} > \mathbf{0}$ and $\text{rank}(\Phi) = k$, and $\mathbf{H} \mathbf{R}_1^{-1} \mathbf{H}^T \geq \mathbf{0}$. Applying the matrix inversion lemma it follows that \mathbf{P}_1 is indeed given by (31) and substituting it in (33) we get:

$$\begin{aligned} \mathbf{W} &= \mathbf{W}_0 - \mathbf{P}_0 \mathbf{H} (\mathbf{R}_1 + \mathbf{H}^T \mathbf{P}_0 \mathbf{H})^{-1} (\mathbf{W}_0^T \mathbf{H})^T + \\ &\quad (\mathbf{P}_0 - \mathbf{P}_0 \mathbf{H} (\mathbf{R}_1 + \mathbf{H}^T \mathbf{P}_0 \mathbf{H})^{-1} \mathbf{H}^T \mathbf{P}_0) \mathbf{H} \mathbf{R}_1^{-1} \mathbf{Z}^T \end{aligned} \quad (34)$$

where $\mathbf{W}_0 = \mathbf{P}_0 \Phi \mathbf{R}^{-1} \mathbf{Y}^T$, $\mathbf{P}_0 = (\Phi \mathbf{R}^{-1} \Phi^T)^{-1}$ is indeed the solution of $\min_{\mathbf{W}} f_0(\mathbf{W})$ based on *Theorem 1*. We can further process the last term in (34), i.e.:

$$\begin{aligned} &(\mathbf{P}_0 - \mathbf{P}_0 \mathbf{H} (\mathbf{R}_1 + \mathbf{H}^T \mathbf{P}_0 \mathbf{H})^{-1} \mathbf{H}^T \mathbf{P}_0) \mathbf{H} \mathbf{R}_1^{-1} \mathbf{Z}^T \\ &= (\mathbf{P}_0 \mathbf{H} - \mathbf{P}_0 \mathbf{H} (\mathbf{R}_1 + \mathbf{H}^T \mathbf{P}_0 \mathbf{H})^{-1} \mathbf{H}^T \mathbf{P}_0 \mathbf{H}) \mathbf{R}_1^{-1} \mathbf{Z}^T \\ &= \mathbf{P}_0 \mathbf{H} (\mathbf{I}_k - (\mathbf{R}_1 + \mathbf{H}^T \mathbf{P}_0 \mathbf{H})^{-1} (\pm \mathbf{R}_1 + \mathbf{H}^T \mathbf{P}_0 \mathbf{H})) \mathbf{R}_1^{-1} \mathbf{Z}^T \\ &= \mathbf{P}_0 \mathbf{H} (\mathbf{R}_1 + \mathbf{H}^T \mathbf{P}_0 \mathbf{H})^{-1} \mathbf{Z}^T \end{aligned} \quad (35)$$

and substituting it back to (34) we arrive at the solution given by (30). ■

Theorem 3: Problem (29) is equivalent to the problem

$$\min_{\mathbf{W}} \text{tr}\{(\mathbf{W} - \mathbf{W}_0) \mathbf{P}_0^{-1} (\mathbf{W} - \mathbf{W}_0)^T\} + \quad (36)$$

$$\text{tr}\{(\mathbf{Z} - \mathbf{W}^T \mathbf{H})^T \mathbf{R}_1^{-1} (\mathbf{Z} - \mathbf{W}^T \mathbf{H})\} \quad (37)$$

where \mathbf{W}_0 , \mathbf{P}_0 are the solution to $\min_{\mathbf{W}} f_0(\mathbf{W})$.

Proof: Taking the gradient and solving w.r.t. \mathbf{W} we can readily obtain (33) after which the same analysis as in the proof of *Theorem 2* follows. ■

Theorem 4: The optimization problem

$$\min_{\mathbf{W}} f_0(\mathbf{W}) \quad (38)$$

$$\text{s.t. } \mathbf{W}^T \mathbf{H} = \mathbf{Z}$$

with $f_0(\mathbf{W}) = \text{tr}\{(\mathbf{Y} - \mathbf{W}^T \bar{\Phi})^T \mathbf{R}^{-1}(\mathbf{Y} - \mathbf{W}^T \bar{\Phi})\}$, $\mathbf{Y} \in \mathbb{R}^{n \times m}$, $\mathbf{W} \in \mathbb{R}^{k \times n}$, $\bar{\Phi} \in \mathbb{R}^{k \times m}$, $\text{rank}(\bar{\Phi}) = k$, $\mathbf{R} \in \mathcal{S}_{++}^n$, $\mathbf{Z} \in \mathbb{R}^{n \times l}$, $\mathbf{H} \in \mathbb{R}^{k \times l}$, $\text{rank}(\mathbf{H}) = l \leq k$, is equivalent to the problem:

$$\min_{\mathbf{W}} f_0(\mathbf{W}) + \text{tr}\{(\mathbf{Z} - \mathbf{W}^T \mathbf{H})^T \mathbf{R}_\epsilon^{-1} (\mathbf{Z} - \mathbf{W}^T \mathbf{H})\} \quad (39)$$

for $\mathbf{R}_\epsilon \rightarrow \mathbf{0}^+$.

Proof: To find the solution of (38) we introduce the Language multipliers $\mathbf{V} \in \mathbb{R}^{n \times l}$ and form the Lagrangian $L(\mathbf{W}, \mathbf{V}) = f_0(\mathbf{W}) + 2\text{tr}\{\mathbf{V}^T (\mathbf{W}^T \mathbf{H} - \mathbf{Z})\}$. The KKT conditions are:

$$\frac{\partial L}{\partial \mathbf{W}} = -\bar{\Phi}(\mathbf{Y} - \mathbf{W}^T \bar{\Phi})^T + \mathbf{H} \mathbf{V} = \mathbf{0} \quad (40)$$

$$\frac{\partial L}{\partial \mathbf{V}} = \mathbf{H}^T \mathbf{W} - \mathbf{Z}^T = \mathbf{0} \quad (41)$$

Solving (40) for \mathbf{W} we get:

$$\mathbf{W} = \mathbf{W}_0 - \mathbf{P}_0 \mathbf{H} \mathbf{V} \quad (42)$$

where $\mathbf{W}_0 = \mathbf{P}_0 \bar{\Phi} \mathbf{Y}^T$, $\mathbf{P}_0 = (\bar{\Phi} \mathbf{R}^{-1} \bar{\Phi}^T)^{-1}$ which is indeed invertible since $\text{rank}(\bar{\Phi}) = k$. Since \mathbf{P}_0 is invertible and $\text{rank}(\mathbf{H}) = l$, i.e. has full column rank, we can substitute (42) in (41) to solve for \mathbf{V} :

$$\mathbf{V} = -(\mathbf{H}^T \mathbf{P}_0 \mathbf{H})^{-1} (\mathbf{Z} - \mathbf{W}_0^T \mathbf{H})^T$$

Substituting the last equation in (42), we obtain the solution:

$$\mathbf{W}_1 = \mathbf{W}_0 + \mathbf{P}_0 \mathbf{H} (\mathbf{H}^T \mathbf{P}_0 \mathbf{H})^{-1} (\mathbf{Z} - \mathbf{W}_0^T \mathbf{H})^T \quad (43)$$

Turning our attention to problem (39) we can apply the result of *Theorem 2* and notice that for $\mathbf{R}_1 = \mathbf{R}_\epsilon \rightarrow \mathbf{0}^+$ we get indeed the same solution as in (43). ■

Theorem 5: Given the solution \mathbf{W}_1 , \mathbf{P}_1 of the problem

$$\min_{\mathbf{W}} f_0(\mathbf{W}) + \text{tr}\{(\mathbf{Z} - \mathbf{W}^T \mathbf{H})^T \mathbf{R}_1^{-1} (\mathbf{Z} - \mathbf{W}^T \mathbf{H})\} \quad (44)$$

with $f_0(\mathbf{W}) = \text{tr}\{(\mathbf{Y} - \mathbf{W}^T \bar{\Phi})^T \mathbf{R}^{-1}(\mathbf{Y} - \mathbf{W}^T \bar{\Phi})\}$, $\mathbf{Y} \in \mathbb{R}^{n \times m}$, $\mathbf{W} \in \mathbb{R}^{k \times n}$, $\bar{\Phi} \in \mathbb{R}^{k \times m}$, $\text{rank}(\bar{\Phi}) = k$, $\mathbf{R}, \mathbf{R}_1 \in \mathcal{S}_{++}^n$, $\mathbf{Z} \in \mathbb{R}^{n \times l}$, $\mathbf{H} \in \mathbb{R}^{k \times l}$, the solution to the problem:

$$\min_{\mathbf{W}} f_0(\mathbf{W}) \quad (45)$$

can be calculated as:

$$\hat{\mathbf{W}}_0 = \mathbf{W}_1 + \mathbf{P}_1 \mathbf{H} (-\mathbf{R}_1 + \mathbf{H}^T \mathbf{P}_1 \mathbf{H})^{-1} (\mathbf{Z} - \mathbf{W}_1^T \mathbf{H})^T \quad (46)$$

$$\hat{\mathbf{P}}_0 = \mathbf{P}_1 - \mathbf{P}_1 \mathbf{H} (-\mathbf{R}_1 + \mathbf{H}^T \mathbf{P}_1 \mathbf{H})^{-1} \mathbf{H}^T \mathbf{P}_1 \quad (47)$$

$$\hat{\mathbf{P}}_0^{-1} = \mathbf{P}_1^{-1} - \mathbf{H} \mathbf{R}_1^{-1} \mathbf{H}^T \quad (48)$$

where $\hat{\mathbf{P}}_0 > \mathbf{0}$.

Proof: Denoting

$$f_1(\mathbf{W}) = f_0(\mathbf{W}) + \text{tr}\{(\mathbf{Z} - \mathbf{W}^T \mathbf{H})^T \mathbf{R}_1^{-1} (\mathbf{Z} - \mathbf{W}^T \mathbf{H})\}$$

it follows that

$$f_0(\mathbf{W}) = f_1(\mathbf{W}) - \text{tr}\{(\mathbf{Z} - \mathbf{W}^T \mathbf{H})^T \mathbf{R}_1^{-1} (\mathbf{Z} - \mathbf{W}^T \mathbf{H})\}$$

We can rewrite $f_1(\mathbf{W})$ as:

$$f_1(\mathbf{W}) = \text{tr}\{(\bar{\mathbf{Y}} - \mathbf{W}^T \bar{\Phi})^T \bar{\mathbf{R}}^{-1} (\bar{\mathbf{Y}} - \mathbf{W}^T \bar{\Phi})\}$$

with

$$\bar{\mathbf{Y}} = [\mathbf{Y}^T \ \mathbf{Z}^T]^T, \ \bar{\Phi} = [\Phi^T \ \mathbf{H}^T]^T, \ \bar{\mathbf{R}} = \text{blkdiag}(\mathbf{R}, \mathbf{R}_1)$$

Minimizing $f_0(\mathbf{W})$ we have:

$$\begin{aligned} \frac{\partial f_0}{\partial \mathbf{W}} &= \frac{\partial (f_1(\mathbf{W}) - \text{tr}\{(\mathbf{Z} - \mathbf{W}^T \mathbf{H})^T \mathbf{R}_1^{-1} (\mathbf{Z} - \mathbf{W}^T \mathbf{H})\})}{\partial \mathbf{W}} = \mathbf{0} \\ (\mathbf{P}_1^{-1} - \mathbf{H} \mathbf{R}_1^{-1} \mathbf{H}^T) \mathbf{W} &= (\bar{\Phi} \bar{\mathbf{R}}^{-1} \bar{\mathbf{Y}}^T - \mathbf{H} \mathbf{R}_1^{-1} \mathbf{Z}^T) \end{aligned} \quad (49)$$

where $P_1^{-1} = \bar{\Phi} \bar{R}^{-1} \bar{\Phi}^T = P_0^{-1} + H R_1^{-1} H^T$ and $P_0^{-1} = \bar{\Phi} R^{-1} \bar{\Phi}^T$. Since $R > 0$ and $\text{rank}(\bar{\Phi}) = k$ it follows that $P_0^{-1} > 0$ which also entails that $P_1^{-1} > 0$ as $R_1 > 0$ and $H R_1^{-1} H^T \geq 0$. Notice also that $(P_1^{-1} - H R_1^{-1} H^T) = P_0^{-1}$ hence we can invert it in (49) to get:

$$W = (P_1^{-1} - H R_1^{-1} H^T)^{-1} (\bar{\Phi} \bar{R}^{-1} \bar{Y}^T + H(-R_1^{-1}) Z^T)$$

Applying the matrix inversion lemma we have:

$$W = W_1 - P_1 H (-R_1 + H^T P_1 H)^{-1} (W_1^T H)^T + (P_1 - P_1 H (-R_1 + H^T P_1 H)^{-1} H^T P_1) H (-R_1^{-1}) Z^T \quad (50)$$

where $W_1 = P_1 \bar{\Phi} \bar{R}^{-1} \bar{Y}^T$, $P_1 = (\bar{\Phi} \bar{R}^{-1} \bar{\Phi}^T)^{-1}$ is indeed the solution of $\min_W f_1(W)$ based on *Theorem 1*. Notice that $-R_1 + H^T P_1 H$ is in fact negative definite, hence it is invertible. To prove so, consider the following matrix:

$$M = \begin{bmatrix} P_1^{-1} & H \\ H^T & R_1 \end{bmatrix}$$

Since $P_1^{-1} > 0$ and the Schur complement of M w.r.t. the upper left block matrix is $P_1^{-1} - H R_1^{-1} H^T = P_0^{-1} > 0$ it follows that $M > 0$ [17]. Therefore, as $R_1 > 0$ and $M > 0$ it should also hold that the Schur complement of M w.r.t. the lower right block matrix should be positive definite, i.e.:

$$R_1^{-1} - H^T P_1 H > 0 \Rightarrow -R_1^{-1} + H^T P_1 H < 0$$

We can further process the last term in (50) similar to the analysis in (35) to find that:

$$(P_1 - P_1 H (-R_1 + H^T P_1 H)^{-1} H^T P_1) H (-R_1^{-1}) Z^T = P_1 H (-R_1 + H^T P_1 H)^{-1} Z^T$$

and substituting the last in (50) we obtain the result given by (46). Finally, having already established that $P_1 > 0$ and $-R_1^{-1} + H^T P_1 H < 0$ it follows that $-P_1 H (-R_1 + H^T P_1 H)^{-1} H^T P_1 \geq 0$ hence $\hat{P}_0 > 0$. ■

REFERENCES

- [1] A. Billard, S. Calinon, R. Dillmann, and S. Schaal, *Robot Programming by Demonstration*. Berlin, Heidelberg: Springer Berlin Heidelberg, 2008, pp. 1371–1394.
- [2] A. J. Ijspeert, J. Nakanishi, H. Hoffmann, P. Pastor, and S. Schaal, “Dynamical movement primitives: Learning attractor models for motor behaviors,” *Neural Comput.*, vol. 25, no. 2, pp. 328–373, Feb 2013.
- [3] L. Kouttras and Z. Doulgeri, “A novel dmp formulation for global and frame independent spatial scaling in the task space,” in *2020 29th IEEE International Conference on Robot and Human Interactive Communication (RO-MAN)*, 2020, pp. 727–732.
- [4] H. Hoffmann, P. Pastor, D. Park, and S. Schaal, “Biologically-inspired dynamical systems for movement generation: Automatic real-time goal adaptation and obstacle avoidance,” in *2009 IEEE International Conference on Robotics and Automation*, 2009, pp. 2587–2592.
- [5] G. Maeda, M. Ewerton, R. Lioutikov, H. B. Amor, J. Peters, and G. Neumann, “Learning interaction for collaborative tasks with probabilistic movement primitives,” in *2014 IEEE-RAS International Conference on Humanoid Robots*, Nov 2014, pp. 527–534.
- [6] G. J. Maeda, G. Neumann, M. Ewerton, R. Lioutikov, O. Kroemer, and J. Peters, “Probabilistic movement primitives for coordination of multiple human–robot collaborative tasks,” *Autonomous Robots*, vol. 41, no. 3, pp. 593–612, Mar 2017. [Online]. Available: <https://doi.org/10.1007/s10514-016-9556-2>
- [7] C. Cardoso, L. Jamone, and A. Bernardino, “A novel approach to dynamic movement imitation based on quadratic programming,” in *2015 IEEE International Conference on Robotics and Automation (ICRA)*, 2015, pp. 906–911.
- [8] A. Paraschos, C. Daniel, J. Peters, and G. Neumann, “Using probabilistic movement primitives in robotics,” *Auton. Robots*, vol. 42, no. 3, p. 529–551, Mar. 2018. [Online]. Available: <https://doi.org/10.1007/s10514-017-9648-7>
- [9] P. Pastor, L. Righetti, M. Kalakrishnan, and S. Schaal, “Online movement adaptation based on previous sensor experiences,” in *2011 IEEE/RSJ International Conference on Intelligent Robots and Systems*, Sept 2011, pp. 365–371.
- [10] A. Gams, A. Ijspeert, S. Schaal, and J. Lenarcic, “On-line learning and modulation of periodic movements with nonlinear dynamical systems,” *Autonomous Robots*, vol. 27, pp. 3–23, 07 2009.
- [11] J. Umlauf, D. Sieber, and S. Hirche, “Dynamic movement primitives for cooperative manipulation and synchronized motions,” in *2014 IEEE International Conference on Robotics and Automation (ICRA)*, 2014, pp. 766–771.
- [12] B. Nemec, A. Gams, M. Deniša, and A. Ude, “Human-robot cooperation through force adaptation using dynamic motion primitives and iterative learning,” in *2014 IEEE International Conference on Robotics and Biomimetics (ROBIO 2014)*, 2014, pp. 1439–1444.
- [13] A. Sidiropoulos and Z. Doulgeri, “A reversible dynamic movement primitive formulation,” in *2021 International Conference on Robotics and Automation (ICRA)*, 2021, pp. ?–?
- [14] A. Sidiropoulos, D. Papageorgiou, and Z. Doulgeri, “A novel framework for generalizing dynamic movement primitives under kinematic constraints,” *Autonomous Robots*, Oct 2022. [Online]. Available: <https://doi.org/10.1007/s10514-022-10067-4>
- [15] T. Kastritsi, D. Papageorgiou, I. Sarantopoulos, Z. Doulgeri, and G. A. Rovithakis, “Stability of active constraints enforcement in sensitive regions defined by point-clouds for robotic surgical procedures,” in *2019 18th European Control Conference (ECC)*, 2019, pp. 1604–1609.
- [16] T. Kailath, A. Sayed, and B. Hassibi, *Linear Estimation*, ser. Prentice-Hall information and system sciences series. Prentice Hall, 2000. [Online]. Available: <https://books.google.gr/books?id=zNJAQAIAIAAJ>
- [17] G. Strang, *Linear algebra and its applications*. Belmont, CA: Thomson, Brooks/Cole, 2006.